Opto-chemo-mechanical transduction in photoresponsive gels elicits switchable self-trapped beams with remote interactions

Derek R. Morim[a,1], Amos Meeks[b,1], Ankita Shastri[c,1], Andy Tran[a], Anna V. Shneidman[b,d], Victor V. Yashin[e], Fariha Mahmood[a], Anna C. Balazs[e], Joanna Aizenberg[b,c,d,2], and Kalaichelvi Saravanamuttu[a,2]

[a]Department of Chemistry and Chemical Biology, McMaster University, ON L8S 4M1, Canada; [b]John A. Paulson School of Engineering and Applied Sciences, Harvard University, Cambridge, MA 02138; [c]Department of Chemistry and Chemical Biology, Harvard University, Cambridge, MA 02138; [d]Kavli Institute for Bionano Science and Technology, Harvard University, Cambridge, MA 02138; and [e]Department of Chemical and Petroleum Engineering, University of Pittsburgh, Pittsburgh, PA 15261

Edited by Samuel I. Stupp, Northwestern University, Evanston, IL, and accepted by Editorial Board Member Tobin J. Marks January 2, 2020 (received for review February 28, 2019)

Next-generation photonics envisions circuitry-free, rapidly reconfigurable systems powered by solitonic beams of self-trapped light and their particlelike interactions. Progress, however, has been limited by the need for reversibly responsive materials that host such nonlinear optical waves. We find that repeatedly switchable self-trapped visible laser beams, which exhibit strong pairwise interactions, can be generated in a photoresponsive hydrogel. Through comprehensive experiments and simulations, we show that the unique nonlinear conditions arise when photoisomerization of spiropyran substituents in pH-responsive poly(acrylamide-*co*-acrylic acid) hydrogel transduces optical energy into mechanical deformation of the 3D cross-linked hydrogel matrix. A Gaussian beam self-traps when localized isomerization-induced contraction of the hydrogel and expulsion of water generates a transient waveguide, which entraps the optical field and suppresses divergence. The waveguide is erased and reformed within seconds when the optical field is sequentially removed and reintroduced, allowing the self-trapped beam to be rapidly and repeatedly switched on and off at remarkably low powers in the milliwatt regime. Furthermore, this opto-chemo-mechanical transduction of energy mediated by the 3D cross-linked hydrogel network facilitates pairwise interactions between self-trapped beams both in the short range where there is significant overlap of their optical fields, and even in the long range—over separation distances of up to 10 times the beam width—where such overlap is negligible.

dynamic optics | photochromic gels | self-trapped beams | nonlinear dynamics | spiropyran

Self-trapped light beams and spatial solitons emerge in a rich variety of photoresponsive materials that display intensity-dependent changes in refractive index (1–4). These nonlinear waves propagate without diverging through self-inscribed waveguides and exhibit intriguingly particlelike interactions such as collisions (5), fusion and birth (6), annihilation (7), and spiraling (8), typically in the short range (where there is significant overlap in their optical fields) and in rare cases, over long distances (where overlap is negligible and beams are remote) (9, 10). Because they travel without changing shape, self-trapped beams hold potential for optical interconnects (11), applications in image transmission (12), rerouting light (13, 14), and logic gates for computing (15). Importantly, they form the basis of the next-generation light-guiding-light approach to optical signal processing, which envisions a circuitry-free, reconfigurable, and multilayered photonics technology powered by the dynamic interactions of self-trapped beams (13, 14). Advances, however, have been limited by the need for robust photoresponsive materials with switchable—rather than irreversible—changes in refractive index, Δn, which would generate the rapidly reconfigurable self-trapped beams and transient waveguide architectures necessary for repeated dynamic interactions. Extensive studies of self-trapped beams in reversibly responsive media such as photorefractive crystals (16), liquid crystals (17), atomic vapor (18), and Kerr media (19) have focused predominantly on steady-state self-trapping conditions due to their generally fast dynamics. Moreover, Δn in these materials can only be generated at large powers (several watts) or in the presence of an external electric field (2, 3, 6–10). While reversible self-trapping of a single relatively low-power beam (25 μW) due to iodide photooxidation has been reported in a gel for two cycles spanning hundreds of seconds, the persistence of triiodide within the sample prevented further cycling (20).

Here we show that reversible opto-chemo-mechanical transduction in a spiropyran (SP)-functionalized hydrogel elicits rapidly switchable self-trapped laser beams at low powers (μW-mW) and facilitates their dynamic, mutually tunable pairwise interactions both in the short range and remotely. Self-trapping in this material originates from the generation of a transient waveguide appearing due

Significance

Self-trapped light beams hold potential for optical interconnects, applications in image transmission, rerouting light, logic gates for computing and, importantly, for the next-generation light-guiding-light signal processing, which envisions a circuitry-free and reconfigurable photonics powered by the dynamic interactions of self-trapped beams. In conventional nonlinear materials, however, self-trapping suffers from either the need for large incident beam powers and loss of beam interactions at large distances, or it is slow and irreversible. We show that rapidly and repeatably switchable self-trapped laser beams with remote communication capabilities can be elicited at exceptionally small intensities in a pliant, processable hydrogel functionalized with a chromophore. The ability to generate self-trapped beams with this unique set of properties offers unprecedented opportunities to develop light-guiding-light technologies.

Author contributions: J.A. and K.S. designed research; D.R.M., A.M., A.S., A.T., and A.V.S. performed research; D.R.M., A.M., A.S., V.V.Y., F.M., A.C.B., and K.S. contributed new reagents/analytic tools; D.R.M., A.M., A.S., A.T., A.V.S., V.V.Y., F.M., A.C.B., J.A., and K.S. analyzed data; and D.R.M., A.M., A.V.S., V.V.Y., J.A., and K.S. wrote the paper.

The authors declare no competing interest.

This article is a PNAS Direct Submission. S.I.S. is a guest editor invited by the Editorial Board.

[1]D.R.M., A.M., and A.S. contributed equally to this work.

[2]To whom correspondence may be addressed. Email: jaiz@seas.harvard.edu or kalai@mcmaster.ca.

This article contains supporting information online at https://www.pnas.org/lookup/suppl/doi:10.1073/pnas.1902872117/-/DCSupplemental.

First published February 6, 2020.

to the reversible laser-initiated isomerization of SP chromophores and concomitant contraction of the host gel in the irradiated region (21, 22). The same mechanism serves as an elegant photoswitch in drug release (23), data storage (24, 25), sensing (26), nanofluidics (27), self-assembly (28), and, when incorporated into polymers (29), enables tuning of stiffness (30), surface wettability (31), and photonic bandgaps (32). Isomerization-related swelling in hydrogels (21, 32, 33) has been used in the design of microfluidics (34), multiresponsive polymers (35), and photocontrollable surface topographies (36) and can be achieved with a variety of photoswitches (37, 38). In these wide-ranging applications, however, photoisomerization is a discrete event with a linear correlation to the photoresponse of the medium. Self-trapping, by contrast, relies on the positive nonlinear feedback between the optical field and nascent refractive index changes in the hydrogel. Our detailed theoretical and experimental results suggest that self-trapping of laser beams in the chromophore-functionalized hydrogel is enabled by the transduction of optical energy to mechanical deformation of the flexible, three-dimensionally (3D) interconnected matrix. Significantly, the deformation is delocalized beyond the incident optical field in the medium, which permits long-range communication between self-trapped beam pairs. These findings address the critical need for rapidly switchable self-trapped beams in soliton-driven photonics such as light-guiding-light computing (24, 25) and opens opportunities in the design of intelligent light-responsive materials such as autonomous light-activatable soft robotics (39), drug-delivery mechanisms (23), and transient waveguide circuitry (14).

Results and Discussion

To generate and study the interactions of self-trapped laser beams, we synthesized a pH-responsive poly(acrylamide-*co*-acrylic acid) (p[AAm-*co*-Aac]) hydrogel containing covalently attached dangling SP moieties (Fig. 1). Details of the synthesis and gel composition are provided in *Materials and Methods*, and *SI Appendix*, section S1 describes the synthesis of the chromophore monomer (*SI Appendix*, section S1.2.1) and its incorporation into cross-linked hydrogels (*SI Appendix*, section S1.2.2.1), non-cross-linked polymer (*SI Appendix*, section S1.2.2.2), and solution samples (*SI Appendix*, section S1.2.3) (21, 22, 40, 41). When immersed in water, the tethered chromophores exist predominantly in the protonated ring-open merocyanine form due to the presence of vicinal acrylate anions (40). When this SP-modified p(AAm-*co*-AAc) gel is irradiated with visible light, the isomerization of merocyanine to its closed-ring SP (1) form triggers a cascade of events, which culminates in a local increase in the refractive index (Δn) of

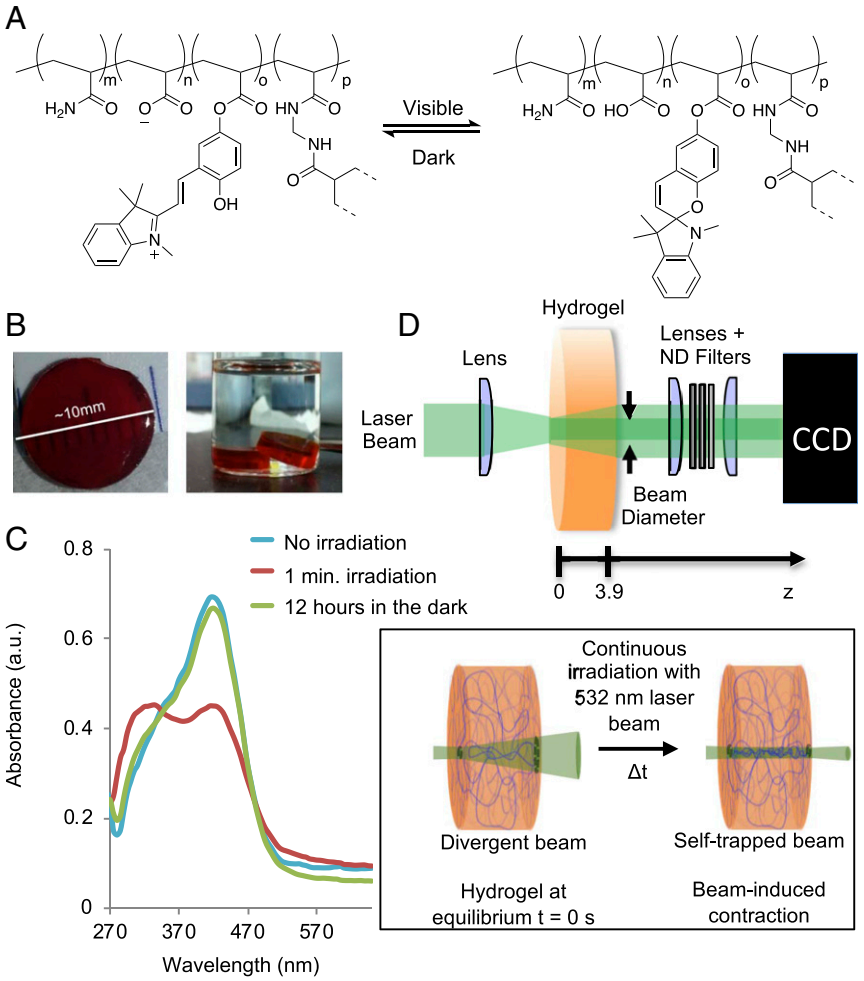

Fig. 1. SP-modified hydrogels. (*A*) Photoisomerization scheme of chromophore substituents from the protonated merocyanine (MCH^+, *Left*) to SP (*Right*) forms in the methylenebis(acrylamide) cross-linked p(AAm-*co*-AAc) hydrogel. (*B*) Photographs of chromophore-containing p(AAm-*co*-AAc) hydrogel monoliths employed in experiments. (*C*) UV-visible absorbance spectra demonstrating reversible isomerization of MCH^+ (absorption λ_{max} = 420 nm) to SP (λ_{max} = 320 nm) in solution. (*D*) Experimental setup (*Top*) to probe laser self-trapping due to photoinduced local contraction of the hydrogel, schematically depicted on the *Bottom* (see also Movie S1). A laser beam is focused onto the entrance face of the hydrogel while its exit face is imaged onto a CCD camera.

the hydrogel. Specifically, the conversion of merocyanine to SP results in an increase in hydrophobicity, which in turn triggers the local expulsion of water and ultimately, contraction of the hydrogel matrix along the irradiated path (22, 33). Detailed theoretical treatment of the light-induced contraction of the hydrogel due to changes in hydrophobicity is provided in *SI Appendix*, section S2.3.1; coupling of the photoisomerization process to gel dynamics is detailed in *SI Appendix*, sections S2.3.2. Evidence for photoisomerization is shown in Fig. 1*C*, where the depletion of the absorbance band (λ_{max} = 420 nm), attributed to the π-π^* electronic transition of the protonated merocyanine, is accompanied by growth of an absorbance band in the UV region (λ_{max} = 320 nm), associated with the π-π^* electronic transition of the chromene moiety in the SP isomer (40). Isomerization is reversible, so that in the absence of visible radiation SP thermally relaxes back to the merocyanine isomer.

Self-Trapping of Visible Laser Light. We exploit the light-triggered contraction and corresponding increase in refractive index, Δn, of the SP-modified p(AAm-*co*-AAc) hydrogel to elicit rapid, efficient, and reversible self-trapping of a visible laser beam. We deliberately selected the 532-nm wavelength for our studies; the relatively low absorbance at this wavelength ensures that the laser beams could propagate through the sample without significant attenuation but also possess sufficient intensity to initiate the ring-closing reaction of the chromophore moieties. The significance of striking a balance in this way between the transparency of the medium and eliciting photoisomerization is detailed in *SI Appendix*, section S2.1.1. In all cases herein, the beam diameter is defined in the conventional way, as twice the axial distance at which the beam intensity drops to $1/e^2$ of its maximum value, and is set to be 20 μm at $z = 0$ mm. Under linear conditions, where there are no photoinduced changes along its path (i.e., at low powers or in the absence of isomerizable chromophores), the beam divergence is calculated to be ∼130 μm for a propagation distance of 3.9 mm through the gel (greatly exceeding the Rayleigh length of 0.6 mm) (4). We anticipated that this natural optical divergence would be strongly suppressed when the beam initiates isomerization of protonated merocyanine moieties and in turn, contraction of the pH-responsive hydrogel along its propagation path (Fig. 1 *D*, *Bottom*). Because this contracted region contains a greater volume fraction of polymer, its refractive index is greater compared to its immediate surroundings, which now contains an increased proportion of water [refractive indices of the polymer and water are $n \sim 1.49$ and $n \sim 1.33$, respectively (42)]. This densified region serves as a cylindrical microscopic waveguide (19, 43–46)—a self-induced optical fiber—that entraps the laser beam as its fundamental optical mode and guides it through the medium without diverging.

Experimental results confirming our hypothesis are shown in Fig. 2. Under linear conditions—in the absence of photoinduced changes—a visible laser beam indeed diverges along the 3.9-mm pathlength to a width of ∼120 μm (in agreement with the calculated value of 130 μm; *SI Appendix*, Fig. S1*D*). When launched through the SP-modified p(AAm-*co*-AAc) hydrogel, the beam self-traps and propagates without diverging indicative of unique nonlinear conditions generated in the gel. The temporal dynamics of the beam is contained in plots of peak intensity and width and corresponding spatial intensity profiles (Fig. 2*A* and *SI Appendix*, section S2.1). Within 50 s, the beam undergoes an ∼20-fold increase in peak intensity from ∼10 to 200% with a concurrent ∼threefold decrease in width from 120 to 40 μm (Fig. 2*A*). With time, the beam continues to increase in relative intensity to 390% with a corresponding decrease in width to 22 μm, which is comparable to its width of 20 μm at the entrance face. This signifies that the self-trapped beam now propagates from the entrance to the exit face with negligible divergence. As detailed in *SI Appendix*, section S2.1.2, these results also show that despite the absorbance inherent to the medium, self-trapping is an efficient process.

We find that self-trapping dynamics depends strongly on optical intensity (Fig. 2*C* and *SI Appendix*, section S2.2 and Fig. S2). Self-trapping efficiency, defined as the greatest percent change in beam width relative to the initial diverged width, increases monotonically from roughly 30 to 80% (with a concomitant decrease in minimum beam width from ∼110 to ∼20 μm) when optical power

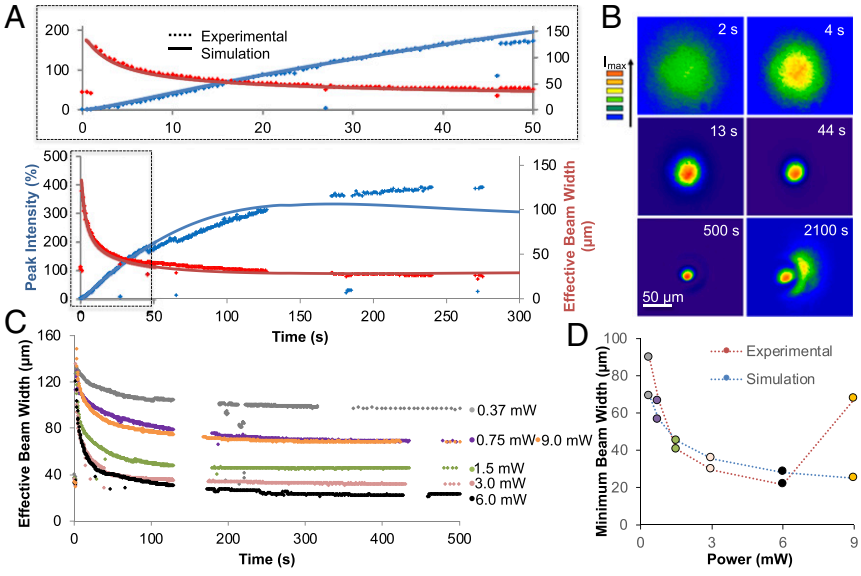

Fig. 2. Evolution of self-trapping in the SP-modified hydrogel; experiments and simulations. (*A*) Experimentally measured temporal evolution of peak intensity (blue) and effective width (red) of a laser beam (532 nm, 6.0 mW, with a width of 20 μm—corresponding peak intensity = 3.77 kW cm^{-2}) acquired at the sample exit face; the beam is turned on at t = 0. Breaks in plots are time lapses between image logs. The experimental plots (dotted lines) are compared to numerical simulations (solid lines); the dashed black box above provides a zoomed-in view from 0 to 50 s, emphasizing the match between the experimental results and simulations. (*B*) Two-dimensional (2D) spatial intensity profiles experimentally acquired at select times. (*C*) Temporal evolution of beam width during self-trapping experiments at different optical powers. (*D*) Comparison of calculated and experimental values of minimum self-trapped beam width as a function of beam power.

was increased from 0.37 to 6.0 mW. However, the efficiency decreased to ∼54% when the power was increased further to 9 mW. These trends were observed in at least nine repeat experiments at each intensity.

To describe and provide insight into the self-trapping process, we developed a numerical model that couples the photoisomerization of chromophores with localized volume changes in the hydrogel; details are provided in *Materials and Methods* and *SI Appendix*, section S2.3. Briefly, the model couples the photoinduced isomerization of SP to the local swelling and contraction of the hydrogel (*SI Appendix*, sections S2.3.1 and S2.3.2) and calculates the resulting impact on light propagation in the medium (*SI Appendix*, sections S2.3.3–S2.3.5) (47–49). As the covalently tethered SP moieties cannot diffuse freely, they are transported with their host polymer chains upon swelling and contraction of the hydrogel. The amount of isomerized SP within a given volume—i.e., its concentration—therefore depends on the flux of polymer chains as well as the optical intensity-dependent rate constant associated with merocyanine-to-SP isomerization and the intensity-independent rate of thermal relaxation of SP to merocyanine. The osmotic pressure induced by the isomerization process leads to a local change in the polymer volume fraction. The corresponding changes in refractive index (Δn) and isomerization-dependent light absorption are calculated and employed in the nonlinear paraxial wave equation to determine the intensity distribution of light within the gel. This distribution of optical intensity is then employed to calculate the isomerization dynamics and associated Δn in the gel. This cycle is repeated iteratively until the desired time is reached.

Consistent with experiments, the model accurately captures the short-term (<500 s) self-trapping dynamics along with the intensity-dependent self-trapping efficiency of a single laser beam in the hydrogel (Fig. 2*A* and *SI Appendix*, Fig. S6). As in experiments, the simulated self-trapping efficiency increases monotonically with beam power spanning 0.37 to 6.0 mW (Fig. 2*D*). This trend originates from the intensity dependence of the photoisomerization process: at lower intensities, the proportion of protonated merocyanine isomerized to SP does not extend far enough into the hydrogel to create the Δn needed for appreciable self-focusing; as the intensity increases, the concentration of isomerized SP molecules rapidly saturates to a plateau in self-trapping efficiency. At the higher intensities, the SP-rich region surrounding the beam leads to contraction of the hydrogel that is large enough to prevent significant divergence of the beam, enabling a greater proportion of the optical energy to extend further into the gel. This triggers more isomerization and thus additional focusing of the beam in a nonlinear feedback loop. At greater powers and longer times, the material exhibits a decrease in self-trapping efficiency due to the excitation of high-order modes (m > 0) (43) as the saturation of isomerization at large intensities forms a flat-top concentration profile that extends beyond the beam width, creating a wider waveguide (*SI Appendix*, Fig. S7).

Reversibility of Self-Trapping. Photoisomerization of merocyanine moieties enables the self-trapped beam to be controllably switched on and off >45 times in the same hydrogel. Temporal plots of relative peak intensity and beam width (Fig. 3) show that after each dark period, the relaunched beam always diverges to ∼120 μm—its original diverged form under linear conditions (*vide supra*). This can only occur if the waveguide previously induced by the self-trapped beam is completely erased and the hydrogel relaxes to its equilibrium state. Accordingly, self-trapping efficiency (ratio of minimum to initially diverged beam width) is consistent between experiments with typical values of 57–65% (corresponding to minimum beam widths of 42–56 μm, respectively).

Mechanism of Self-Trapping. We elucidated the mechanistic origins of reversible self-trapping in the hydrogel through a carefully designed series of control experiments (Fig. 4) in conjunction with numerical simulations. Experiments involving p(AAm-*co*-AAc) gel without chromophore (Fig. 4*A*); solution of free SP without a gel (Fig. 4*B*); p(AAm-*co*-AAc) hydrogel dispersed with untethered SP molecules (Fig. 4*C*); and non-pH–responsive poly (hydroxyethyl)methacrylate p(AAm-*co*-HEMA) hydrogel with covalently bound SP (Fig. 4*D*) all exhibited negligible or significantly suppressed self-trapping compared to the pH-responsive p(AAm-*co*-AAc) incorporating covalently bound SP (the rationale for the selection of the control systems and detailed discussions of results are provided in *SI Appendix*, section S2.4 and Figs. S8–S10). These studies, further supported by time-dependent UV-visible spectroscopy (described in *SI Appendix*, Fig. S11 *A–C* and section S2.5) and fluorescence recovery after photobleaching measurements (described in *SI Appendix*, Fig. S11 *D* and *E* and section S2.6), show that all of the following features are critical for creating the nonlinear conditions required for efficient self-trapping: 1) the photoisomerization, 2) presence of a gel network, 3) chromophore tethering, and 4) acidic moieties on the polymer backbone,

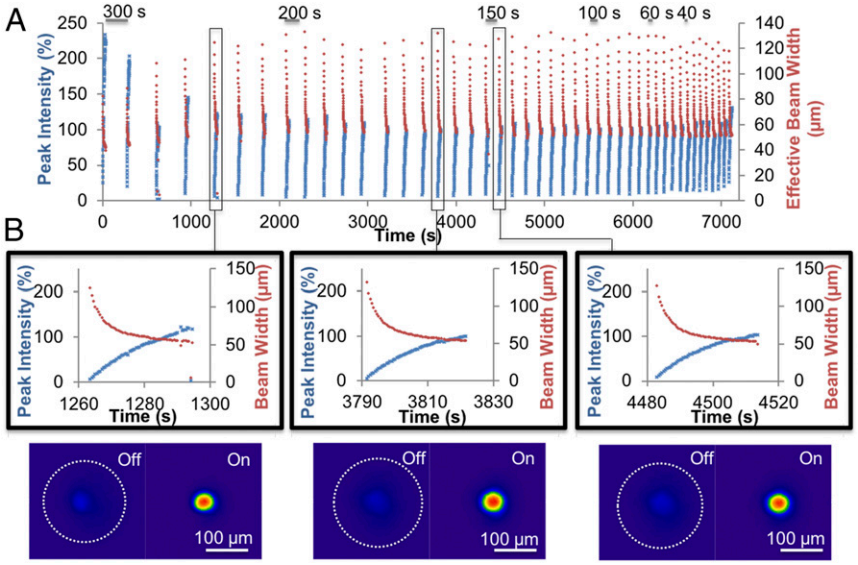

Fig. 3. Rapidly reversible self-trapping in the SP-modified p(AAm-*co*-AAc). (*A*) Temporal plots of peak intensity (blue) and effective diameter (red) over 45 cycles of self-trapping of a laser beam. Cycles of 30 s were separated by dark periods ranging from 300 to 40 s (indicated above the plots). (*B*) Scheme and spatial intensity profiles showing the "off" (divergent) and "on" (self-trapped) states of the laser beam over select cycles. White circles trace the diameter ($1/e^2$) of the initially divergent beam in the off state.

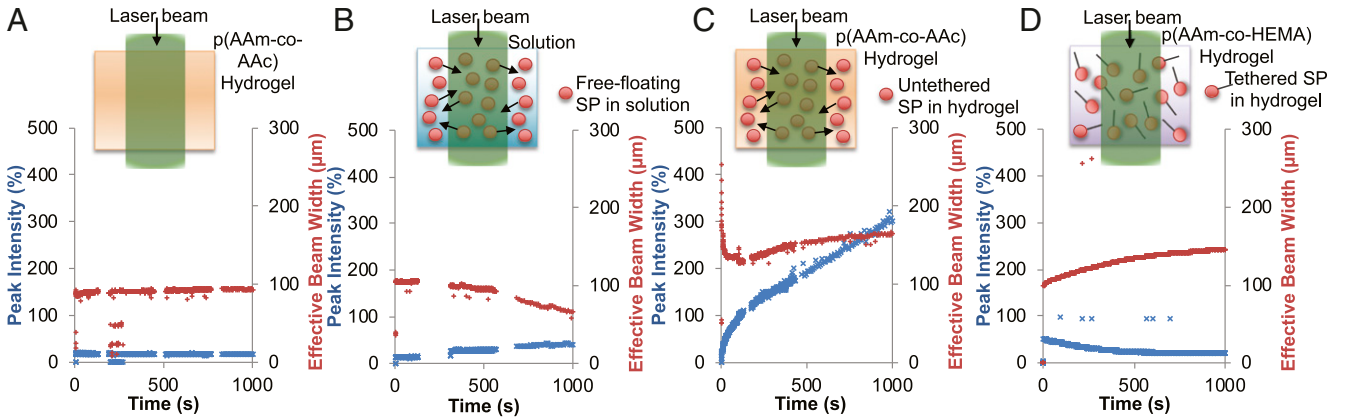

Fig. 4. Self-trapping in control systems; experimental measurements. Temporal plots of peak intensity (blue) and width (red) of a laser beam acquired at the exit face of (*A*) an unmodified p(AAm-*co*-AAc) hydrogel, (*B*) solution of SP in DMSO:water, (*C*) p(AAm-*co*-AAc) hydrogel dispersed with untethered SP, and (*D*) SP-modified poly (hydroxyethyl)methacrylate p(AAm-*co*-HEMA) hydrogel. Laser power of 9 mW (5.65 kW cm^{-2}) was employed in *A* and 6.0 mW (3.77 kW cm^{-2}) in *B*–*D*.

supporting the hypothesis that self-trapping originates from a sequence of events triggered by the photoisomerization of the merocyanine isomer and consequent contraction of the pH-responsive hydrogel (22, 34, 40, 48). These control studies also confirmed that any local heating by the incident laser beam was not sufficient to elicit self-trapping. Instead, they confirmed that self-trapping originates from the transduction of optical-to chemical-to mechanical energy, which is most efficient and reversible when the chromophore units are covalently tethered to the 3D interconnected hydrogel (Fig. 2).

Remote Interactions of a Parallel Pair of Self-Trapped Beams. We found that a self-trapped beam could be dynamically and reciprocally controlled by launching a second, parallel-propagating counterpart into the medium. Remarkably, this communication between the self-trapped beam pair occurs remotely—even over separation distances (Δx) that greatly exceed (by at least 10-fold) the widths of either self-trapped beam. This behavior is significant because the interactions between self-trapped beams typically rely on the overlap of the optical fields and therefore decrease exponentially with Δx. For example, it has been shown that self-trapped beams in a photopolymer did not interact when separated by four times the beam width (45). Although there are multiple examples of nonlocal photoresponses based on the diffusion of heat, matter, or charge carriers, there are only two previous experimental examples of long-range interactions between self-trapped beams (9, 10). This was achieved in a liquid crystal system where cooperative motion of liquid crystals extended the index changes outside of the light field (9), but only under an externally applied electric field. Nonlocal interactions were also achieved in a thermally conductive lead glass. In the latter, the diffusion of heat extended the photoresponse outside of the optical field (10), but only at optical intensities that were three orders of magnitude greater than those employed in our study.

Interactions between self-trapped beams in our material are 1) facilitated by the reversible photoresponse and 2) mediated through the 3D interconnected, flexible network of the hydrogel. The former enables a self-trapped beam to rapidly alter its intensity profiles in response to a second beam. The latter enables the two self-trapped beams to communicate even when overlap between their optical fields is negligible. Temporal plots of relative intensity capture the rich internal dynamics of two identical and parallel beams propagating through the SP-modified p(AAm-*co*-AAc) hydrogel; Δx in these experiments ranged from ∼25 to ∼200 μm (limited only by the experimental assembly), which were 1.25–10 times larger, respectively, than the input beam diameter of 20 μm (Fig. 5 and *SI Appendix*, Fig. S12). To enable ease of comparison of the interacting beams, the intensity of each beam in these studies was scaled to its initial intensity and reported as a dimensionless ratio termed relative peak intensity; such plots trace the dynamics of each beam when its counterpart is blocked for some time (Fig. 5 *A* and *B*, *Left*). At all values of Δx, the beams self-trapped significantly to widths of ∼20 μm individually (Fig. 2 and *SI Appendix*, Fig. S12) but mutually suppressed self-trapping efficiency when propagating together. Spatial intensity profiles of the two beams acquired at different times during these cycles highlight the differences between single and copropagating self-trapped beams (Fig. 5 *A* and *B*, *Right*). By measuring the self-trapping rates of two beams introduced sequentially into the hydrogel, we further show that there is strong reciprocal correlation between the photoinduced Δn (and therefore, the extent of contraction) between the two remote regions of the hydrogel (*SI Appendix*, Fig. S12 and section S3.1).

Initial numerical simulations of the dynamics of two proximal beams (Δx = 25 μm) confirm that all of the experimentally observed behaviors are strongly influenced by photoinduced deformation of the hydrogel network (Fig. 5*C* and *SI Appendix*, Fig. S13 and Movie S3; for detailed discussion of simulation results, see *SI Appendix*, section S3.2). As the gel contracts along the propagation path of the beam, expelled solvent causes the surrounding matrix to swell. Competition arises when a second self-trapped beam induces contraction in a neighboring region. Solvent is now expelled by both beams leading to opposing forces of expansion so that at early times (20 s), the beams briefly repel each other. Simultaneous self-trapping prevents either beam from eliciting the maximum possible Δn and therefore, neither beam is able to attain its optimum self-trapping efficiency. Simulated beams launched simultaneously attain a minimum width of ∼35 μm (*SI Appendix*, Fig. S13), and when one beam is removed, the other decreases in width to ∼20 μm and doubles in relative peak intensity—behavior consistent with experiments. A full and detailed understanding of how the beams communicate in this material at longer separation distances, which includes consideration of local heating effects, will be the subject of future work (*SI Appendix*, section S3.2). Regardless of the mechanism, these unique interactions between self-trapped beams in a photoresponsive hydrogel reveal intriguing dynamics for optically modulating beams of light.

Conclusions

We showed that rapidly switchable and strongly interacting self-trapped beams of visible laser light can be elicited in a soft, easily

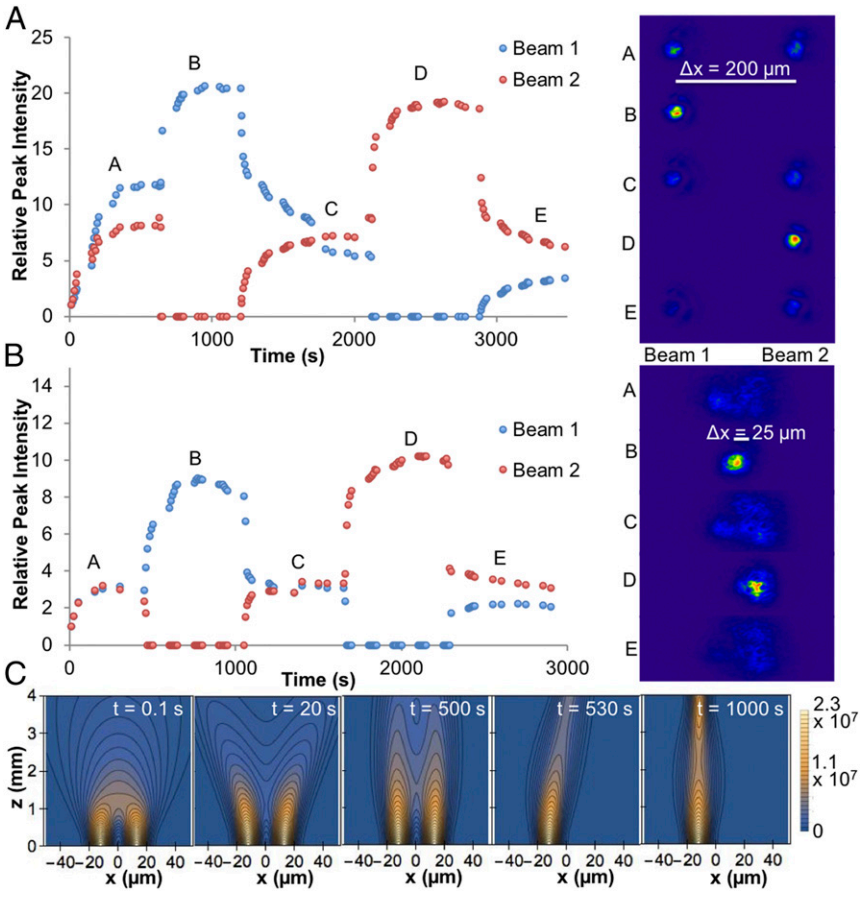

Fig. 5. Dynamic interactions of two parallel self-trapped beams. (*A*) Temporal plots of relative peak intensities (*Left*) and corresponding 2D spatial intensity profiles (*Right*) acquired at select times at the sample exit face for two beams separated by Δx = ~200 μm. When propagating together, beam 1 (blue) and beam 2 (red) self-trapped over 625 s to a relative peak intensity of 12 and 9, respectively (from an initial value of 1), and comparable widths of ~40 μm (labeled as region A on the plot and intensity profile; details in *SI Appendix*, section S3.1). When beam 2 was selectively blocked, beam 1 rapidly returned to high self-trapping efficiency, increasing in relative intensity to ~20 with a minimum width of ~28 μm over 250 s (labeled as region B). When beam 2 was reintroduced, however, beam 1 diminished in self-trapping efficiency, decreasing in relative peak intensity to 5.3 and broadening again to ~40 μm over 800 s; beam 2 also showed reduced efficiency, attaining a maximum relative peak intensity of only 7 and a width of ~40 μm (region C). The equivalent effect was observed when beam 1 was blocked in the next cycle of the same experiment (region D). (*B*) Temporal plots of relative peak intensities and corresponding 2D spatial intensity profiles for two beams separated by Δx = 25 μm. (*C*) Simulations snapshots of the interactions of two self-trapped beams with Δx = 25 μm. Color shows the intensity in Wm^{-2}. See also *SI Appendix*, Figs. S12 and S13 and Movies S2 and S3.

processable hydrogel functionalized with a chromophore. Our material system relies on the photoisomerization of SP moieties, which is extensively employed as a binary "on–off" photoswitching mechanism (40). We showed that the same isomerization process can serve as the conduit that transduces optical energy through reversible chemical transformations into mechanical forces in the gel, which in turn generate unique nonlinear conditions required for self-trapping. More specifically, a visible laser beam self-traps by initiating isomerization of photoacidic merocyanine substituents tethered to a p(AAm-*co*-AAc) hydrogel network. The concomitant change in hydrophobicity of the polymer chain results in the local expulsion of water, contraction of the gel, and consequent increase in refractive index (Δn). This creates a reciprocal, positive feedback between the optical field and nascent Δn along its propagation path, thus generating a transient waveguide. When the optical field is removed, isomerization is reversed, and the hydrogel relaxes to its original state; in this way, the self-trapped beam is reversibly and reproducibly switched on and off by sequentially removing and reintroducing the Gaussian beam. Intriguingly, interactions between beams extend well beyond the confines of the incident optical field in this material. As a result of this nonlocal response, a pair of parallel-propagating self-trapped beams exhibits strong, mutually responsive interactions in the short and long range. Our theoretical model provides valuable mechanistic insight into these interactions, by coupling photoisomerization to osmotic-pressure-driven contraction of the gel.

In conventional nonlinear materials (1–4, 16–19), self-trapping suffers from one or more of the following disadvantages: 1) the need for large incident beam powers (~watt) (19), 2) presence of an external field (16, 17), 3) loss of beam interactions at distances beyond the overlap of their electromagnetic fields (2, 13), and 4) it is slow and irreversible (11, 45). In contrast, the presented materials system demonstrates highly efficient self-trapping 1) at small, easily accessible (~milliwatt) beam powers, 2) under ambient conditions; it is 3) rapid (~50 s), 4) fully reversible at relatively fast timescales (~100 s), and shows 5) sustained repeatability over multiple cycles (at least ~50) and 6) almost instantaneous beam interactions for separation distances up to 10 beam widths. These exceptional properties are enabled by the large Δn created by gel contraction, reversibility of photochemical reactions (i.e., chromophore isomerization), and 3D interconnectivity of a polymer network. Importantly, our study elucidates an opto-chemo-mechanical transduction pathway to elicit nonlinear optical conditions in a photochromic hydrogel. Although its switching speeds are considerably smaller than the typically < nanosecond timescales of optoelectronic switches, our system provides proof of concept and lays the foundation for rational design of other classes of faster-responding photochromic hydrogels. For example, in *SI Appendix*, section S4, we present preliminary simulations of the effect of poroelastic diffusion and chromophore isomerization on self-trapping dynamics. These results suggest that photoisomerization kinetics of the chromophore plays the principal role in determining the photoresponse time. Indeed, the system presented in this study carries rich opportunities for optimization of photoresponse time through the chemical design of the chromophore and hydrogel medium, and modulation of the optical fields to control the shape and intensity of the incident beams. Regardless of switching speed, such photochromic hydrogels also hold promise as rewritable optical media for self-modulating beams. The possibility to reversibly modulate beams of visible light remotely at relatively low powers opens the door to all-optical computing with ambient light (24, 25), autonomous stimuli-responsive soft robotic systems (39) and

actuators for a wide range of applications including drug delivery (23), and dynamic optics (40).

Materials and Methods

See *SI Appendix* for additional experimental details.

Preparation of Hydrogel Samples. The polymerizable hydrogel matrix was prepared by dissolving acrylamide:acrylic acid or acrylamide:2-hydroxyethyl methacrylate (HEMA) in a mixture of dimethyl sulfoxide (DMSO):deionized water before addition of the cross-linker. Acrylated SP (for tethered samples) or hydroxyl-substituted SP was then added to the unpolymerized hydrogel matrix followed by an addition of a catalyst. Hydrogel samples were cured in a circular plastic mold (d = 10 mm, h = 4 mm thick).

Optical Experiments. Self-trapping experiments were carried out on an optical assembly that focused either one or two beams (continuous wave [c.w.], 532 nm, d = 20 μm) onto the entrance window of the cell containing the hydrogel sample (*SI Appendix*, Fig. S1 *C* and *E*). The spatial intensity profile of the beam(s) at the exit face of the cell was imaged by a planoconvex lens pair onto a charge-coupled device (CCD) camera. Additional details of optical experiments are provided in *SI Appendix*, section S2.1.

Simulations. *SI Appendix*, section S2.3 provides details of the model employed for simulations. Briefly, a Gaussian beam is launched into the medium that initially has a uniform refractive index profile. The intensity-dependent rate of photoisomerization leads to corresponding changes in local osmotic pressures, calculated by solving the linearized equations of gel dynamics (47). Changes in the refractive index (Δn) originating from changes in the volume fraction of polymer chains are then input into the nonlinear equation for the complex amplitude of the light wave to simulate the resulting modified distribution of light intensity in the medium. In this way, the rate equations for photoisomerization, osmotic-pressure-induced gel deformation, and optical intensity are solved iteratively until a steady state is reached.

Data Availability. The data that support the findings of this study are available in the main text and *SI Appendix*. Additional information is available from the corresponding authors upon reasonable request.

ACKNOWLEDGMENTS. This work was supported by the US Army Research Office under Award W911NF-17-1-0351 and by the Natural Sciences and Engineering Research Council, Canadian Foundation for Innovation, and McMaster University. A.M. was supported by the Department of Defense through the National Defense Science & Engineering Graduate Fellowship Program. We acknowledge the participation of Dr. Liqun Qiu in preliminary experiments. We thank Dr. Ian B. Burgess for suggesting that self-trapping could occur in photochromic hydrogels and Dr. Michael M. Lerch for discussions.

1. S. Biria, D. R. Morim, F. An Tsao, K. Saravanamuttu, I. D. Hosein, Coupling nonlinear optical waves to photoreactive and phase-separating soft matter: Current status and perspectives. *Chaos* **27**, 104611 (2017).
2. G. I. Stegeman, M. Segev, Optical spatial solitons and their interactions: Universality and diversity. *Science* **286**, 1518–1523 (1999).
3. R. Y. Chiao, E. Garmire, C. H. Townes, Self-trapping of optical beams. *Phys. Rev. Lett.* **13**, 479–482 (1964).
4. S. Trillo, W. Torruellas, *Spatial Solitons* (Springer, New York, 2001).
5. A. W. Snyder, A. P. Sheppard, Collisions, steering, and guidance with spatial solitons. *Opt. Lett.* **18**, 482–484 (1993).
6. W. Królikowski, S. A. Holmstrom, Fusion and birth of spatial solitons upon collision. *Opt. Lett.* **22**, 369–371 (1997).
7. W. Królikowski, B. Luther-Davies, C. Denz, T. Tschudi, Annihilation of photorefractive solitons. *Opt. Lett.* **23**, 97–99 (1998).
8. A. V. Buryak, Y. S. Kivshar, M.-f. Shih, M. Segev, Induced coherence and stable soliton spiraling. *Phys. Rev. Lett.* **82**, 81–84 (1999).
9. M. Peccianti, K. A. Brzdkiewicz, G. Assanto, Nonlocal spatial soliton interactions in nematic liquid crystals. *Opt. Lett.* **27**, 1460–1462 (2002).
10. C. Rotschild, B. Alfassi, O. Cohen, M. Segev, Long-range interactions between optical solitons. *Nat. Phys.* **2**, 769–774 (2006).
11. S. Jradi, O. Soppera, D. J. Lougnot, Fabrication of polymer waveguides between two optical fibers using spatially controlled light-induced polymerization. *Appl. Opt.* **47**, 3987–3993 (2008).
12. J. Yang, P. Zhang, M. Yoshihara, Y. Hu, Z. Chen, Image transmission using stable solitons of arbitrary shapes in photonic lattices. *Opt. Lett.* **36**, 772–774 (2011).
13. Y. Kivshar, Spatial solitons: Bending light at will. *Nat. Phys.* **2**, 729–730 (2006).
14. A. W. Snyder, F. Ladouceur, Light guiding light: Letting light be the master of its own destiny. *Opt. Photonics News* **10**, 35–39 (1999).
15. M. Peccianti, C. Conti, G. Assanto, A. De Luca, C. Umeton, All-optical switching and logic gating with spatial solitons in liquid crystals. *Appl. Phys. Lett.* **81**, 3335–3337 (2002).
16. M. F. Shih *et al*., Two-dimensional steady-state photorefractive screening solitons. *Opt. Lett.* **21**, 324–326 (1996).
17. C. Conti, M. Peccianti, G. Assanto, Observation of optical spatial solitons in a highly nonlocal medium. *Phys. Rev. Lett.* **92**, 113902 (2004).
18. J. E. Bjorkholm, A. A. Ashkin, cw self-focusing and self-trapping of light in sodium vapor. *Phys. Rev. Lett.* **32**, 129–132 (1974).
19. A. Ashkin, J. M. Dziedzic, P. W. Smith, Continuous-wave self-focusing and self-trapping of light in artificial Kerr media. *Opt. Lett.* **7**, 276–278 (1982).
20. D. R. Morim, I. Vargas-Baca, K. Saravanamuttu, Reversibly trapping visible laser light through the catalytic photo-oxidation of I(-) by Ru(bpy)3(2+). *J. Phys. Chem. Lett.* **7**, 1585–1589 (2016).
21. K. Sumaru, T. Takagi, S. Sugiura, T. Kanamori, "Spiropyran-functionalized hydrogels" in *Soft Actuators*, K. Asaka, H. Okuzaki, Eds. (Springer, Tokyo, 2014), pp. 219–229.
22. B. Ziółkowski, L. Florea, J. Theobald, F. Benito-Lopez, D. Diamond, Self-protonating spiropyran-Co-NIPAM-Co-acrylic acid hydrogel photoactuators. *Soft Matter* **9**, 8754–8760 (2013).
23. R. Tong, H. D. Hemmati, R. Langer, D. S. Kohane, Photoswitchable nanoparticles for triggered tissue penetration and drug delivery. *J. Am. Chem. Soc.* **134**, 8848–8855 (2012).
24. A. D. Hudson, M. R. Ponte, F. Mahmood, T. Pena Ventura, K. Saravanamuttu, A soft photopolymer cuboid that computes with binary strings of white light. *Nat. Commun.* **10**, 2310 (2019).
25. J. Andréasson *et al*., All-photonic multifunctional molecular logic device. *J. Am. Chem. Soc.* **133**, 11641–11648 (2011).
26. J. Ren, H. Tian, Thermally stable merocyanine form of photochromic spiropyran with aluminum ion as a reversible photo-driven sensor in aqueous solution. *Sensors (Basel)* **7**, 3166–3178 (2007).
27. M. Zhang *et al*., Light and pH cooperative nanofluidic diode using a spiropyran-functionalized single nanochannel. *Adv. Mater.* **24**, 2424–2428 (2012).
28. C. Maity, W. E. Hendriksen, J. H. van Esch, R. Eelkema, Spatial structuring of a supramolecular hydrogel by using a visible-light triggered catalyst. *Angew. Chem. Int. Ed. Engl.* **54**, 998–1001 (2015).
29. L. Florea, D. Diamond, F. Benito-Lopez, Photo-responsive polymeric structures based on spiropyran. *Macromol. Mater. Eng.* **297**, 1148–1159 (2012).
30. E. Samoylova *et al*, Photoinduced variable stiffness of spiropyran-based composites. *Appl. Phys. Lett.* **99**, 201905 (2011).
31. J. Wang, Y. Han, Tunable multiresponsive methacrylic acid based inverse opal hydrogels prepared by controlling the synthesis conditions. *Langmuir* **25**, 1855–1864 (2009).
32. M. Kamenjicki Maurer, I. K. Lednev, S. A. Asher, Photoswitchable spirobenzopyran-based photochemically controlled photonic crystals. *Adv. Funct. Mater.* **15**, 1401–1406 (2005).
33. B. Ziółkowski, L. Florea, J. Theobald, F. Benito-Lopez, D. Diamond, Porous self-protonating spiropyran-based NIPAAm gels with improved reswelling kinetics. *J. Mater. Sci.* **51**, 1392–1399 (2016).
34. S. Sugiura *et al*., Photoresponsive polymer gel microvalves controlled by local light irradiation. *Sens. Actuators A Phys.* **140**, 176–184 (2007).
35. E. U. Kulawardana, T. Kuruwita-Mudiyanselage, D. C. Neckers, Dual responsive poly (N-Isopropylacrylamide) hydrogels having spironaphthoxazines as pendant groups. *J. Polym. Sci. A Polym. Chem.* **47**, 3318–3325 (2009).
36. J. E. Stumpel *et al*., Photoswitchable ratchet surface topographies based on self-protonating spiropyran-NIPAAM hydrogels. *ACS Appl. Mater. Interfaces* **6**, 7268–7274 (2014).
37. X. Su, I. Aprahamian, Hydrazone-based switches, metallo-assemblies and sensors. *Chem. Soc. Rev.* **43**, 1963–1981 (2014).
38. M.-M. Russew, S. Hecht, Photoswitches: From molecules to materials. *Adv. Mater.* **22**, 3348–3360 (2010).
39. L. Hines, K. Petersen, G. Z. Lum, M. Sitti, Soft actuators for small-scale robotics. *Adv. Mater.* **29**, 1603483 (2017).
40. R. Klajn, Spiropyran-based dynamic materials. *Chem. Soc. Rev.* **43**, 148–184 (2014).
41. V. M. Breslin, N. A. Barbour, D.-K. Dang, S. A. Lopez, M. A. Garcia-Garibay, Nanosecond laser flash photolysis of a 6-nitroindolinospiropyran in solution and in nanocrystalline suspension under single excitation conditions. *Photochem. Photobiol. Sci.* **17**, 741–749 (2018).
42. Polymer Properties Database. Chemical Retrieval on the Web (2015). http://polymerdatabase.com/home.html. Accessed 24 January 2020.
43. A. B. Villafranca, K. Saravanamuttu, An experimental study of the dynamics and temporal evolution of self-trapped laser beams in a photopolymerizable organosiloxane. *J. Phys. Chem. C* **112**, 17388–17396 (2008).
44. S. Shoji, S. Kawata, A. A. Sukhorukov, Y. S. Kivshar, Self-written waveguides in photopolymerizable resins. *Opt. Lett.* **27**, 185–187 (2002).
45. R. Malallah *et al*., Controlling the trajectories of self-written waveguides in photopolymer. *J. Opt. Soc. Am. B* **35**, 2046–2056 (2018).
46. Y. S. Kivshar, G. P. Agrawal, *Optical Solitons* (Academic Press, 2003).
47. V. V. Yashin, A. C. Balazs, Theoretical and computational modeling of self-oscillating polymer gels. *J. Chem. Phys.* **126**, 124707 (2007).
48. T. Satoh, K. Sumaru, T. Takagi, T. Kanamori, Fast-reversible light-driven hydrogels consisting of spirobenzopyran-functionalized poly (N-isopropylacrylamide). *Soft Matter* **7**, 8030–8034 (2011).
49. M. Hammarson, J. R. Nilsson, S. Li, T. Beke-Somfai, J. Andréasson, Characterization of the thermal and photoinduced reactions of photochromic spiropyrans in aqueous solution. *J. Phys. Chem. B* **117**, 13561–13571 (2013).